

Electrical Spin Injection and Transport in Semiconductor Spintronic Devices

B.T. Jonker, S.C. Erwin, A. Petrou, and A.G. Petukhov

Abstract

Semiconductor heterostructures that utilize carrier spin as a new degree of freedom offer entirely new functionality and enhanced performance over conventional devices. We describe the essential requirements for implementing this technology, focusing on the materials and interface issues relevant to electrical spin injection into a semiconductor. These are discussed and illustrated in the context of several prototype semiconductor spintronic devices, including spin-polarized light-emitting diodes and resonant tunneling structures such as the resonant interband tunneling diode.

Keywords: ferromagnetic materials, semiconductors, spin injection, spin-polarized materials, spintronics.

Introduction

The field of semiconductor electronics is based exclusively on the manipulation of charge. The phenomenal progress in increasing circuit performance by reducing device dimensions at a rate commonly referred to as Moore's law is likely to be curtailed by practical and fundamental limits by the year 2010.¹ Consequently, there is keen interest in exploring new avenues and paradigms for future technologies. Since an electron bears *spin* as well as charge, combining carrier spin as a new degree of freedom with the established bandgap engineering of modern devices offers exciting opportunities for new functionality and performance, as the other articles in this issue have discussed. This approach is referred to as "semiconductor spintronics."² Materials research and the physics of new spin-dependent phenomena play key roles in this rapidly growing field as researchers work to develop new materials, such as ferromagnetic semiconductors, and try to understand the basic

issues of spin injection and scattering at heterointerfaces.

One may distinguish two broad regimes envisioned for spin-dependent device operation: one in which the net spin polarization is the key parameter (i.e., there are more spins oriented in a given direction than in the opposite direction in either current or number density) and a second in which spin phase coherence is important. This article will focus on the former,³ while the latter is relevant to other avenues of research such as the development of spin-based quantum computation, which relies on the controlled entanglement of wave functions.⁴

One of the earliest proposals for a semiconductor spintronic device was for a spin-polarized field-effect transistor (spin-FET),⁵ in which the source and drain contacts are ferromagnetic materials intended to inject and detect spin-polarized electrons transported in a high-mobility channel. The conductance of the FET would depend on

electron spin orientation in the channel, which would be controlled by the gate voltage relative to the magnetization of the drain contact, producing a spin-based mode of operation. If the magnetization of the source and drain are independently controlled using techniques developed for magnetic memory, such a device offers nonvolatile and reprogrammable operation with spin or magnetization as a virtual fourth terminal, providing additional functionality and a new level of operation. This and other device concepts, including spin-dependent resonant tunneling diodes (spin-RTDs),^{6–11} gated spin coherent devices,^{12,13} spin-polarized light-emitting diodes (spin-LEDs),¹⁴ and tunnel magnetoresistive devices,¹⁵ have stimulated tremendous interest in this rapidly growing field.

There are four essential requirements for implementing a semiconductor spintronics technology in devices:

1. efficient electrical injection of spin-polarized carriers into the semiconductor,
2. adequate spin diffusion lengths and lifetimes for transport within the device,
3. effective control and manipulation of the spin system, and
4. efficient detection of the spin system to determine the output.

Very encouraging progress has been made in the latter three areas. Spin diffusion lengths of many microns^{16,17} and spin lifetimes of >100 ns^{18,19} have been reported in optically pumped GaAs, for example. A number of successful methods have been demonstrated to manipulate^{9,12,13} and detect^{7,14,16,20–23} the state of the spin system. However, an efficient and practical means of electrical spin injection has heretofore been unavailable, and this lack has been a critical issue severely hampering progress in this field.

Electrical Spin Injection: The Spin-LED

Electrical spin injection requires a contact material and a corresponding interface that facilitates the transport of spin-polarized carriers into the semiconductor. The spin-LED¹⁴ shown schematically in Figure 1a is a relatively simple device that enables one to focus on the injection process. Spin-polarized carriers injected from the contact radiatively recombine in the semiconductor, in this case, an AlGaAs/GaAs(001) quantum well (QW). If the carriers retain their spin polarization, the light emitted is circularly polarized. The quantum selection rules that describe the radiative recombination process provide a direct and fundamental link between the circular polarization of the light emitted along the surface normal, P_{circ} , and the spin polarization of the carriers, P_{spin} .^{24,25} For the GaAs QW considered here, $P_{\text{spin}} = P_{\text{circ}}$.

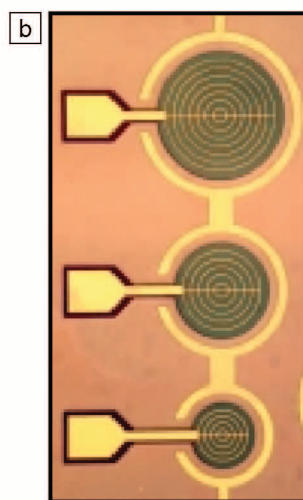
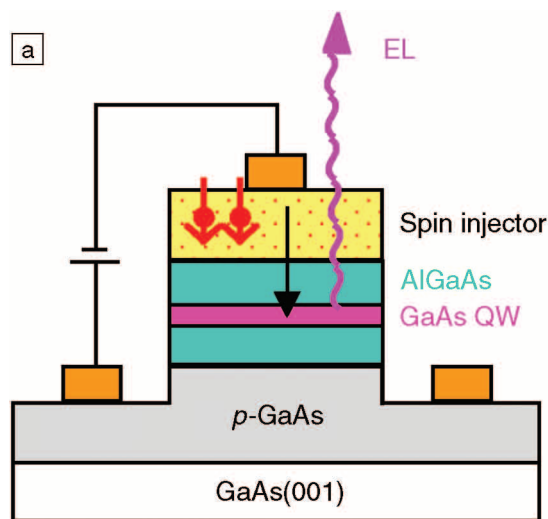


Figure 1. (a) Schematic cross section of a spin-polarized light-emitting diode (spin-LED) for electron injection based on an AlGaAs/GaAs quantum well (QW). EL indicates the surface-emitted electroluminescence. (b) Photograph of an operational spin-LED device. The active mesa areas are 400 μm , 300 μm , and 200 μm in diameter.

while for bulk GaAs, $P_{\text{spin}} = 2P_{\text{circ}}$. Hence, the spin-LED provides a *quantitative* and *model-independent* measure of the carrier spin polarization achieved in the semiconductor due to injection from any contact/interface. Note that this non-time-resolved measurement provides a lower bound for P_{spin} since the spin lifetime in the QW is typically shorter than the radiative lifetime. The helicity of the emitted light may be switched simply by changing the magnetization of the contact. Practical utilization of the spin-LED may include integrated chemical sensors or polarization-encoded optical information transfer. A photograph of an operational spin-LED is shown in Figure 1b.

Magnetic Semiconductor Contacts

A semiconductor that exhibits a net spin polarization is an ideal candidate for the injecting contact, since one can then design the structure using the established principles of bandgap engineering (in particular, the known band offsets) to optimize spin injection across the heterointerface. A *semimagnetic semiconductor* such as $\text{Zn}_{1-x}\text{Mn}_x\text{Se}$ is attractive for a number of reasons. These strongly paramagnetic materials exhibit a giant Zeeman effect (the band edges split into discrete spin levels in an applied magnetic field),^{26,27} so that the spin polarization can be continuously tuned by an applied magnetic field to provide an essentially 100% spin-polarized electron population, although only at relatively low temperatures. $\text{Zn}_{1-x}\text{Mn}_x\text{Se}$ is a well-studied material closely lattice-matched to GaAs, and the interface is well behaved and under-

stood. Finally, it can readily be doped *n*-type, allowing one to focus on *electron* transport, which is the basis for modern high-frequency device technology. The first reports of electrical spin injection from such contacts into a GaAs QW LED showed large circular polarization ($\sim 50\%$) of the raw electroluminescence data, convincingly demonstrating that the electrons reaching the QW were spin-polarized.^{28–30}

An example of such data is shown in Figure 2, where the electroluminescence (EL) is plotted as a function of photon energy and analyzed for positive ($\sigma+$) and negative ($\sigma-$) helicity. P_{circ} is defined as the difference in intensity of these components divided by their sum. At zero applied field, no optical polarization is observed, as expected. However, in an applied field, the giant Zeeman splitting of the $\text{Zn}_{1-x}\text{Mn}_x\text{Se}$ conduction band produces a highly polarized electron population that is injected into the AlGaAs/GaAs QW. Radiative recombination with unpolarized holes injected from the *p*-type buffer layer results in the spectra shown. The large difference in intensity between the $\sigma+$ and $\sigma-$ components is the signature of a spin-polarized carrier population in the QW, as clearly shown by the selection rules, which determine the radiative transitions allowed by quantum mechanical conservation of momentum (inset in Figure 2). Thus, a simple inspection of the raw data confirms successful electrical spin injection. The polarization of the EL data shown is 72% and saturates at a value of 83% for higher fields.³ The quantum selection rules provide a quantitative link between P_{circ} and the

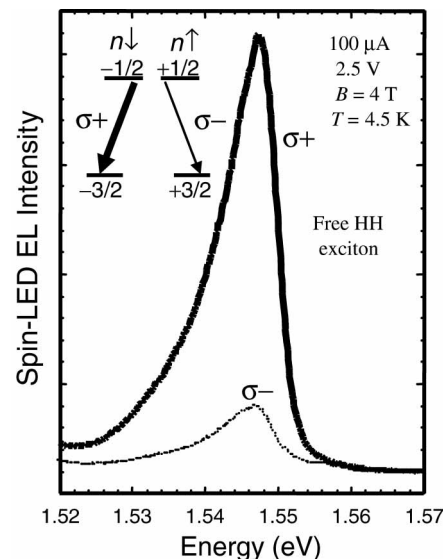


Figure 2. Electroluminescence data (Faraday geometry) from a surface-emitting LED with a $\text{Zn}_{0.94}\text{Mn}_{0.06}\text{Se}$ contact analyzed for $\sigma+$ and $\sigma-$ polarization for an applied magnetic field $B = 4\text{ T}$. The energy of the EL confirms that recombination occurs in the quantum well via the heavy hole (HH) exciton. For the data shown, $P_{\text{circ}} = 72\%$. The inset shows the radiative HH interband transitions and corresponding optical polarizations allowed by the selection rules $\Delta m_j = \pm 1$. The light hole levels are shifted to higher energy by quantum confinement and do not participate at low temperature.

electron spin polarization: $P_{\text{circ}} = P_{\text{spin}} = (n_{\uparrow} - n_{\downarrow}) / (n_{\downarrow} + n_{\uparrow}) = 0.83$, or 83%, where n_{\uparrow} ($m_j = +1/2$) and n_{\downarrow} ($m_j = -1/2$) are the populations of the electron spin states with quantum number m_j .

These results demonstrate that robust electrical spin injection indeed occurs in an all-semiconductor heterostructure, even across the heterovalent II–VI/III–V interface. Subsequent work has shown that such effects persist across *air-exposed* interfaces following epitaxial regrowth of the $\text{Zn}_{1-x}\text{Mn}_x\text{Se}$ contact.³¹ Analysis of the interface defect structure has further shown that specific defects, such as stacking faults, limit spin-injection efficiency in diffusive transport.³² Such generic defects are a potential source of spin-polarization loss for semiconductor spintronic devices in general and must be considered in device design.

Since semimagnetic semiconductors are paramagnetic, they exhibit significant carrier spin polarization only at low temperatures and high magnetic fields and are not suitable for practical applications. In contrast, ferromagnetic semiconductors (FMSs) exhibit spontaneous ferromagnetic order

at finite temperature and offer many new opportunities. New compounds based on III–V hosts such as $\text{Ga}_{1-x}\text{Mn}_x\text{As}$ are especially exciting because they can be grown on device substrates and incorporated into an existing technology. The basic properties, materials issues, and outlook are described in the article by Dietl and Ohno elsewhere in this issue. Advances in materials quality have increased the Curie temperature of $\text{Ga}_{1-x}\text{Mn}_x\text{As}$ to ~ 150 K, with the potential of exceeding room temperature. Since Mn acts as an acceptor in a III–V host, the III–Mn–V materials are *p*-type—indeed, a high hole density is believed necessary to mediate the ferromagnetic order.^{33,34} Although holes have lower mobilities and much shorter spin lifetimes than electrons, successful spin injection has been observed in carefully tailored structures. Carrier spin polarizations of 6%³⁵ and 1%³⁶ have been reported in spin-LED structures using GaMnAs as the injecting contact. Single-barrier GaMnAs/AlAs/GaMnAs tunneling magnetoresistance (TMR) structures have exhibited changes in resistance of 70% at 8 K for very thin (~ 1.6 nm) AlAs barriers.³⁷ A TMR value of 30% was observed at 4.2 K in an unusual GaMnAs/5 nm AlAs/MnAs structure.³⁸

FMS materials that exhibit *n*-type behavior are especially attractive, since electron transport forms the basis for high-frequency device operation. Very recent work has demonstrated epitaxial growth of a classic FMS, *n*-type CdCr_2Se_4 , on substrates of immediate technological relevance such as GaAs and GaP, although spin transport across the heterointerface has yet to be demonstrated.³⁹ In addition, *n*-type behavior has been reported in a number of other materials believed to be ferromagnetic semiconductors, as discussed in the articles by Dietl and Ohno and by Chambers and Farrow elsewhere in this issue. However, further work is needed to determine if the ferromagnetic behavior observed is a property of the diluted host lattice, as would be the case for a true FMS material, or the result of unwanted precipitates. The detection of spin-polarized band carriers provides an excellent litmus test to distinguish the two.

Magnetic Metal Contacts

Ferromagnetic metals offer most of the properties desired for a practical spin-injecting contact material: a source of electrons rather than holes, high Curie temperatures, low coercive fields, and a well-developed materials technology due to decades of investment largely by the recording industry. Metallization is a standard process in any semiconductor-device fabrication line, thus the use of a ferro-

magnetic metallization could easily be incorporated into existing processing schedules.

A number of groups have attempted to inject spin-polarized carriers from a ferromagnetic metal contact into a semiconductor and reported measured effects on the order of 0.1–1%, with an estimate of actual spin polarization in the semiconductor extracted from a particular model.^{20,40–42} These experiments measured a change in resistance or potential, which some argue may be compromised by contributions from anisotropic magnetoresistance or a local Hall effect.^{43–45}

Recent model calculations by several groups^{45–49} have indicated that the large difference in conductivity between a metal and semiconductor severely inhibits spin injection—the spin-injection coefficient, $\gamma \approx \sigma_N/\sigma_F \ll 1$, is very small, where σ_N and σ_F are the conductivities of the normal (semiconductor) and ferromagnetic (metal) materials, respectively. In an overly simplistic picture, the ability of the semiconductor to accept carriers is independent of spin and much smaller than that of the metal to deliver them. Consequently, equal numbers of spin-up and spin-down electrons are injected regardless of the metal's initial polarization, resulting in essentially zero spin polarization in the semiconductor. This is described in more detail in the appendix accompanying this article (see p. 746), using an equivalent resistor model network. In the diffusive-transport regime (where all existing devices operate), successful spin injection occurs only for two conditions: either the conductivities of the ferromagnetic contact material and semiconductor are closely matched, or the contact is 100% polarized.⁴⁶ If neither condition is satisfied, the spin polarization in the semiconductor is very low ($< 1\%$). No ferromagnetic metal meets either of these criteria. Half-metallic materials offer 100% spin polarization in principle,^{50,51} although defects such as antisites or interface structure rapidly suppress this value.⁵² These results underscore the attraction of ferromagnetic semiconductors.

It was suggested that this obstacle of conductivity mismatch could be circumvented if the interface resistance dominates, for example, by insertion of a tunnel barrier between the metal and semiconductor.^{45,53} The physical principles were first elucidated theoretically by Rashba,⁵³ who noted that such an approach supported a difference in chemical potential between the spin-up and spin-down bands at the interface, thereby enabling the use of ferromagnetic metals as spin-injecting contacts. Various oxides are commonly used as tunnel barriers. Magnetic metal/ Al_2O_3 /metal

structures have been extensively studied, since they form the basis for a tunneling spectroscopy used to determine the metal spin polarization⁵⁴ and for TMR devices being developed for nonvolatile memory.^{55,56}

However, for a metal contact on a semiconductor, the bending of the conduction- and valence-band edges resulting from carrier depletion, which leads to Schottky barrier formation, provides a very natural potential barrier, as shown in Figure 3. For moderately doped semiconductors ($n \sim 10^{16}$ – 10^{18} cm^{-3}), the depletion width is hundreds of angstroms⁵⁷ and very little electron current flows from the metal under reverse bias, characteristic of a rectifying contact. However, this width may be readily controlled by an appropriate doping profile—heavily doping the surface of the semiconductor during molecular-beam epitaxial growth reduces the depletion width to tens of angstroms,⁵⁸ so that tunneling from the metal into the semiconductor becomes a highly probable process. This approach avoids the use of a discrete barrier layer and the accompanying problems with pinholes (holes that occur in the barrier layer and act as electrical shorts), and Schottky contacts are already routine ingredients in semiconductor technology.

This tailored Schottky tunnel barrier approach was successfully demonstrated by Hanbicki et al. using an epitaxial Fe film on an AlGaAs/GaAs QW spin-LED heterostructure,^{59,60} and electron spin polarizations of 32% were achieved in the GaAs QW. The LED structures were grown using an AlGaAs contact-layer doping profile designed to enhance tunneling. EL data from surface-emitting devices were obtained and analyzed as described earlier.^{3,59,60} EL spectra from such a device are shown in Figure 3a as a function of magnetic field. In this case, the field is necessary to align the Fe magnetization (carrier spins) along the surface normal (Faraday geometry), so that the familiar quantum selection rules can be applied. The spectra are dominated by the QW heavy hole (HH) exciton, with a linewidth of 5 meV. HH refers to the valence-band state with the larger effective mass, which in this system lies at lowest energy and therefore dominates the optical transitions at low temperature. At zero field, the σ^+ and σ^- EL components are equal, as expected, since the easy magnetization axis of the Fe film lies in plane. As the Fe magnetization is rotated out of plane, the σ^+ component dominates and a pronounced difference in intensities is observed in the raw data, signaling successful electrical spin injection. The circular polarization directly tracks the out-of-plane magnetization of the Fe film obtained by independent magnetom-

etry measurements, as shown in Figure 3b, and saturates at 32% at a magnetic-field value characteristic of the Fe contact, $2.2T = 4\pi M_{Fe}$, where M_{Fe} is the bulk magnetization of Fe. A number of control ex-

periments show that spurious effects such as dichroism in the Fe film are negligible.⁵⁹

This behavior unambiguously confirms that the spin-polarized electrons recombining in the GaAs QW are electrically injected from the Fe contact, producing a QW spin polarization $P_{spin} = P_{circ} = 32\%$. The sign of P_{circ} confirms that Fe majority-spin electrons dominate,³ consistent with previous work on Fe/Al₂O₃/Al tunnel structures.⁵⁴ Significant polarization is observed to nearly room temperature. Preliminary analysis of the temperature dependence of P_{circ} shows that it is dominated by that of the QW spin lifetimes,⁵⁹ indicating that the injection process is independent of temperature, as expected for tunneling. Detailed analysis of the I - V behavior using the Rowell criteria (three characteristics that the I - V behavior should exhibit if tunneling is occurring), observation of phonon signatures, and a pronounced zero-bias anomaly in the conductance spectra convincingly show that tunneling is the dominant transport mechanism.⁶⁰

The spin-injection efficiency across the Fe/AlGaAs Schottky interface depends strongly on the details of the doping profile at the interface and elsewhere in the structure. Undoped QWs were used in all of the results described to avoid dilution of the electron-spin population and minimize electron-hole interactions, which reduce spin lifetimes. The high n -doping of the AlGaAs surface layer was just sufficient to reduce the width of the depletion layer to a thickness expected to enhance tunneling, while much lower doping levels ($n \sim 10^{16}$ – 10^{17} cm³) were used elsewhere. Heavy doping of extended regions reduces spin injection, due to spin scattering. A detailed model of the role of doping and other parameters is provided by Albrecht and Smith.⁶¹

Zhu et al. also utilized a reverse-biased Schottky barrier to examine spin injection from Fe films grown epitaxially on a GaAs/InGaAs QW structure.⁶² Although they observe no large differences in EL intensity when analyzed for $\sigma+$ and $\sigma-$ polarization, by using pulsed current injection and examining the wings of the Gaussian-like EL spectrum to distinguish the HH exciton contribution, they concluded that an injected spin polarization of $\sim 2\%$ had been realized that was independent of temperature. The reasons for the smaller effect are not clear, although it may be due to lower n -doping in the GaAs at the Fe interface, resulting in a wider barrier and reduced probability for tunneling. This group has also reported 6% injected polarization using a ferromagnetic MnAs metal contact.⁶³

Other groups have recently reported successful spin injection from a ferromagnetic metal into an AlGaAs/GaAs LED structure using a discrete Al₂O₃ layer as the tunnel barrier. Manago and Akinaga obtained spin polarizations of $\sim 1\%$ using either Fe, Co, or NiFe contacts.⁶⁴ Motsnyi et al.⁶⁵ used a CoFe contact and the oblique Hanle effect⁶⁶ to measure and analyze the EL and determined a lower bound of 9% at 80 K for the injected electron spin polarization. This compares favorably to the results for the Schottky tunnel contact.

Fundamental Issues of Interfaces and Spin Injection

A number of groups have explored theoretically the prospects for spin injection across both metal/semiconductor and magnetic/nonmagnetic semiconductor interfaces. In this section, some of the fundamental criteria for injection are sketched, and the results of some specific first-principles computational studies are summarized.

Most theoretical treatments begin by assuming an ordered interface, so that the electron momentum parallel to the interface plane, $k_{||}$, is conserved (i.e., $k_{||}$ is a good quantum number). This approximation is well justified for interfaces between materials whose lattice constants are nearly equal, including certain materials systems of technological interest—such as Fe/GaAs. It also simplifies the formalism most often used for calculating the spin-dependent conductance, the Landauer–Büttiker approach.^{67,68} In this method, the spin-polarized conductance Σ_{σ} is identified with the total transmission probability T_{σ} through the available conducting channels for each spin σ separately:

$$\Sigma_{\sigma} = (e^2/h)T_{\sigma}, \quad (1)$$

where e is the electron charge and h is Planck's constant. By assumption, $k_{||}$ is a good quantum number, and hence the total transmission probability can be written as a sum over the two-dimensional Brillouin zone of the transmission through individual channels labeled by $k_{||}$,

$$T_{\sigma} = \sum_k T_{\sigma}(k_{||}). \quad (2)$$

Methods for calculating $T_{\sigma}(k_{||})$ generally follow the Green's function formalism of Baranger and Stone.⁶⁹ These are numerically intensive approaches whose description is beyond the scope of this review; for more details, see References 70–73.

Although the full computation of Equation 2 is important for numerically accurate results, considerable insight into the important physics can be gained by con-

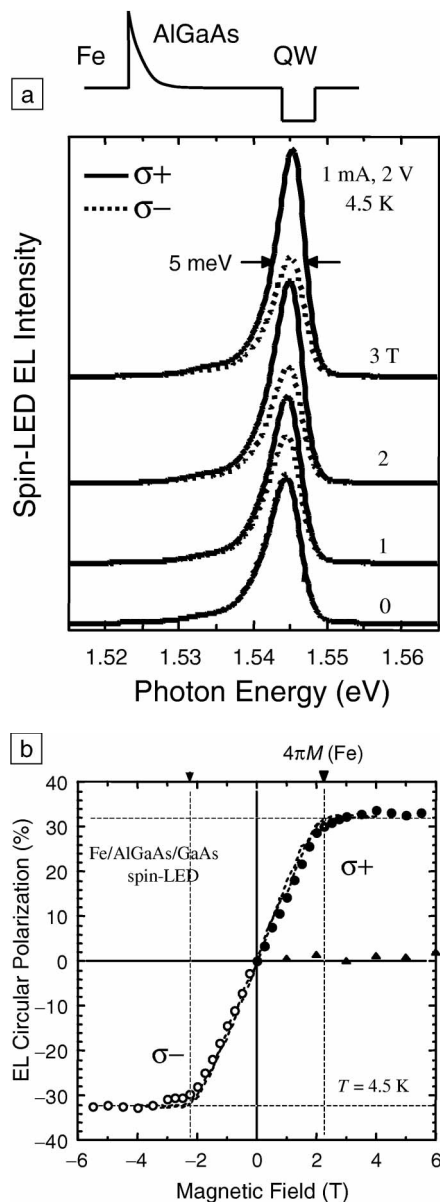


Figure 3. (a) Schematic illustration of the Schottky tunnel barrier that forms at the Fe/AlGaAs interface (conduction-band edge). EL spectra are shown at selected magnetic fields and $T = 4.5$ K. (b) Field-dependence of P_{circ} (open and solid circles) and the out-of-plane component of the Fe film magnetization (dashed line, normalized to the maximum value of P_{circ}). The solid triangles show the contribution to P_{circ} due to magnetic dichroism in the Fe film measured with photoluminescence. This contribution is $\sim 1\% \pm 1\%$.

sidering transmission at the zone center, $T_o(k_{||} = 0)$. This is because the conductance is then controlled by the requirement that the symmetries of the bands in the metal must be compatible with those of the semiconductor. For wave vectors normal to the interface plane, this symmetry matching requirement is particularly easy to analyze. Taking Fe/GaAs as an example, Wunnicke and co-workers⁷² have shown that the full solution of Equation 2 predicts nearly ideal spin-filtering behavior, with spin polarization of the injected current as high as 99%. This result is just what is expected from the fundamental requirement of band-symmetry matching. Specifically, the lowest GaAs conduction bands have the symmetry of the Δ_1 irreducible representation within the C_{2v} group that describes the zinc-blende lattice with a (001) interface. Transmission can only take place from Fe bands whose symmetry group is compatible with $\Delta_1(C_{2v})$; this includes the Fe Δ_1 and Δ_2 bands, but not the Δ_2 or Δ_5 bands. Moreover, the transmission is dominated by the channel between GaAs Δ_1 bands (with s -like symmetry) and Fe Δ_1 bands (with d_{z^2} symmetry). The Fe minority-spin Δ_1 band is more than 1 eV above the Fermi level, while the majority-spin Δ_1 crosses the Fermi level. Hence, for heterojunctions without a tunneling barrier or a Schottky barrier, nearly all of the transport is expected to occur via the majority-spin channel—as borne out by the detailed numerical solution of Equation 2 and as measured experimentally.³

Treating Fe/GaAs as a barrierless interface is a convenient starting point for theoretical treatment, but in practice this interface is known to have a Schottky barrier of 0.6–0.9 eV. Wunnicke et al.⁷² simulated the effect of a Schottky barrier in Fe/GaAs by adding a potential step between the Fe and GaAs; the height of this barrier was fixed and its thickness was varied between 20 Å and 350 Å. The calculated spin polarization of the current was essentially unchanged from the 99% result obtained for barrierless interfaces. This need not always be the case, however; for Fe/ZnSe interfaces, thicker Schottky barriers reduced the spin polarization to about 77%. Nevertheless, these theoretical results for Fe/GaAs are very encouraging for the continuing experimental efforts to demonstrate large spin-injection efficiencies from magnetic metals into semiconductors.

Finally, we briefly discuss what is known about the atomic structure of metal/semiconductor interfaces. Even interfaces between two closely lattice-matched materials may have a nonideal interface structure, with potentially significant consequences for spin transport. Previous

experimental work, summarized in References 3 and 74, has indicated that the Fe/GaAs interface is quite abrupt at the atomic scale, as illustrated in the transmission electron microscopy image in Figure 4.⁷⁵ However, if a small amount of Fe diffuses into the GaAs side of the interface ($\sim 10^{20} \text{ cm}^{-3}$), each such Fe atom will likely carry a local magnetic moment oriented randomly with respect to the magnetization direction and will scatter electrons between the two different spin channels, thereby degrading the injected spin polarization.

It is important to ask, then, whether Fe diffuses into GaAs because it is energetically preferable to do so (in which case it may not be possible to prevent), or because of aspects of the growth process that could be changed, if necessary. A starting point for addressing this issue is to determine, from first principles, the lowest-energy structure of the Fe/GaAs interface. Erwin et al. have taken some preliminary steps in this direction.⁷⁶ Using density functional theory, they analyzed two complementary viewpoints: (1) that the structure of Fe/GaAs is determined by the initial stages of growth, which are controlled by the energetics of Fe adsorption on the GaAs substrate; and (2) that the Fe/GaAs interface can attain its lowest-energy equilibrium configuration regardless of the growth history. For the initial growth stages, they found that the bonding between Fe and As dominated the nucle-

ation of Fe films, to the extent that excess Ga in the surface layer would be displaced by the adsorbing Fe. Under the assumption of equilibrium conditions, they found that intermixed interfaces were favored for Fe films of less than 1–2 monolayers, while abrupt films were favored for more than 2 monolayers. Although neither limit is likely to describe the real interface completely, an important lesson learned was that local chemistry competes with other more nonlocal contributions to the energy. Elucidation of the actual interface structure(s) will have to await further experimental and theoretical investigations.

Modeling More Complex Device Structures

Rashba's theory of spin injection,⁵³ which follows earlier work by van Son et al.⁷⁷, is based on the diffusion approximation and assumes a tunnel contact between the ferromagnet and semiconductor that is *spin-selective*—that is, it has different conductivities for up and down spins—and spin relaxation is neglected. The results highlight two requirements for efficient spin injection: (1) the mesoscopic contact (interface) resistance must dominate, and (2) the contact (interface) must be spin-selective (see the sidebar article for details).

Rashba's theory elucidates several key issues, but the simplifying assumptions that were made lead to certain limitations. First, microscopic calculations of the contact resistances are quite challenging, even in the ballistic limit. In reality, the Landauer–Büttiker formalism should be modified, because the tunnel junction is embedded in a diffusive region.⁷⁸ Second, the theory neglects spin–orbit interactions near the interface. Third, it is limited to the ohmic regime, while in reality, large biases often lead to nonlinear I – V characteristics.

Nevertheless, the theory provides simple and physically sound guidance on how to increase spin-injection efficiencies—for example, by increasing the spin-selectivity of the contact resistance. In principle, any tunnel contact between a ferromagnetic material and a nonmagnetic material will be spin-selective, because the spin polarization of the density of states leads to spin polarization of the tunnel current. While the density of states is not explicitly present in the Landauer formula, it can be shown that the transmission coefficient is proportional to the product of the densities of states in the emitter and collector.⁷⁹ Therefore, one obvious way to improve spin injection is to use highly spin-polarized, or even half-metallic, ferromagnetic emitters.

Most ferromagnetic materials, however, are not half-metallic, and therefore, alter-

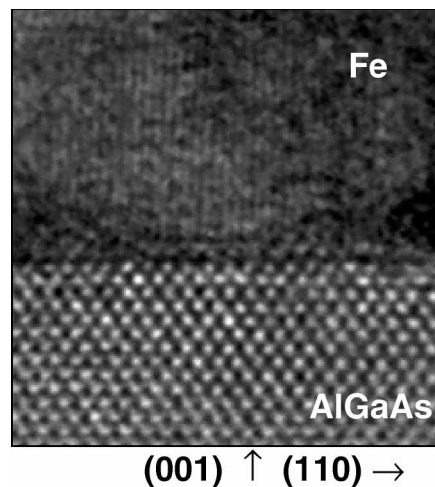


Figure 4. Transmission electron microscopy (TEM) cross-sectional image of the Fe/AlGaAs interface of a spin-LED as described in the article. The vertical lines in the Fe are the fringes corresponding to the (110) planes separated by 2.03 Å. (Courtesy of R.M. Stroud, U.S. Naval Research Laboratory.)

native strategies are important. Here, we discuss two: (1) spin-injection from a ferromagnetic emitter through a specially designed interface into a nonmagnetic collector, and (2) spin-filtering using a magnetically active “interface” such as a ferromagnetic QW. In this design, the interface has an intrinsic spin-selectivity, eliminating the need for a ferromagnetic metal electrode. In the remainder of this section, we discuss these two device designs in more detail.

Spin Injection Using a Specially Designed Interface

Spin-dependent resonant tunneling can be used to increase the spin selectivity of tunneling contacts in a very efficient way. For example, double-barrier heterostructures (DBHs), consisting of a nonmagnetic semiconductor QW between two insulating barriers and two FMS electrodes (see Figure 5 inset), may behave as half-metallic junctions if the parameters of the QW and barriers are properly tuned.¹⁵ Experiments on spin-RTDs reveal a remarkable interplay of magnetism, spin-orbit coupling, and quantum confinement, resulting in pronounced spin-selectivity that can be controlled by an external bias or magnetic field.^{7,80}

Under certain conditions, the spin-RTD is an almost ideal spin valve, allowing tunneling in the majority-spin channel only. The basic physics is easily illustrated with a one-band model.^{15,81} The model is re-

stricted to the ballistic regime and small biases, where only electrons at the Fermi surface contribute to the tunneling current. The geometric parameters of the DBH shown in Figure 5 are tuned so that at $k_{||} = 0$, the resonant level E_R is in the energy interval $0 < E_R < \Delta_{ex}/2$, where Δ_{ex} is the FMS exchange splitting. In this interval, the density of states for the minority spins in the emitter is zero. Therefore, only majority spins can tunnel resonantly from the ferromagnetic emitter. The system works as an almost ideal spin valve even though the ferromagnetic leads are not half-metallic. Within the one-band model, the magnetoresistance grows exponentially with the barrier width and displays a strong maximum as a function of the QW width, reaching a maximum of several thousand percent. This result has no resemblance with the Jullière formula,⁸² since TMR is controlled by the parameters of the nonmagnetic parts of the junction rather than by the spin polarization of the leads. The resonant enhancement of TMR survives even if we take into account spin-flip processes caused by the spin-orbit interaction. For more realistic multi-band calculations, the predicted magnetoresistance is smaller but still very large, reaching 800% for tunneling of holes in GaMnAs/AlAs/GaAs/AlAs/GaMnAs DBHs (Figure 5).^{15,83} Such structures may be used as nonvolatile memory elements or reprogrammable logic gates and incorporated in more complex architectures such

as application-specific integrated circuits or field-programmable gate arrays.

Spin-Filtering Using a Magnetically Active Interface

Electrons in III-V semiconductors have remarkably long spin lifetimes, while the holes rapidly dissipate their spin.¹⁷ Unfortunately, all known III-V FMS materials are *p*-type, and hence only supply spin-polarized holes. For this reason, using interband (or Zener) tunneling is a necessary logical step toward designing all-semiconductor spin-injection devices.^{35,36} Indeed, spin-injection devices based on Zener tunneling of valence electrons from *p*-type ferromagnetic GaMnAs into *n*-GaAs produce injected electron populations with spin polarizations of 1–6%.^{35,36} The band diagram for a recently proposed spin resonant interband tunneling device (spin-RITD) is shown in the inset to Figure 6.⁸⁴ The band offset between InAs and the ferromagnetic GaMnSb QW creates an energy gap between the bottom of the InAs conduction band and the top of the GaMnSb valence band. Therefore, unpolarized electrons from the InAs emitter can tunnel into the InAs collector through hole states in the GaMnSb QW. Since the hole states in the QW are spin-polarized, the emerging electrons will be as well.

Theoretical *I*-*V* characteristics for the spin-RITD are shown in Figure 6a.⁸⁴ The perpendicular spin polarization of the tunneling current is remarkably high, up to

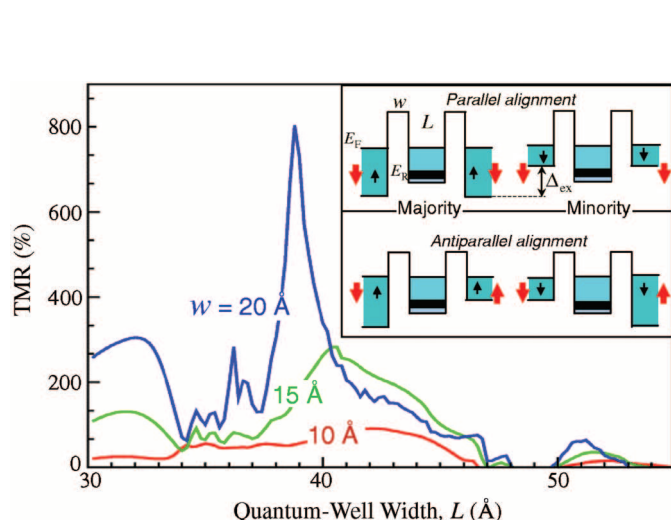


Figure 5. Tunneling magnetoresistance (TMR) of GaMnAs/AlAs/GaAs-based double-barrier heterostructure as a function of the quantum-well width L . Inset: schematic flat-band diagrams illustrating the resonant spin-valve effect. E_F is the Fermi energy, E_R is the resonant level at $k_{||} = 0$, w is the barrier width, and Δ_{ex} is the exchange splitting. Red arrows indicate magnetizations in the leads; black arrows indicate spin of the electrons.

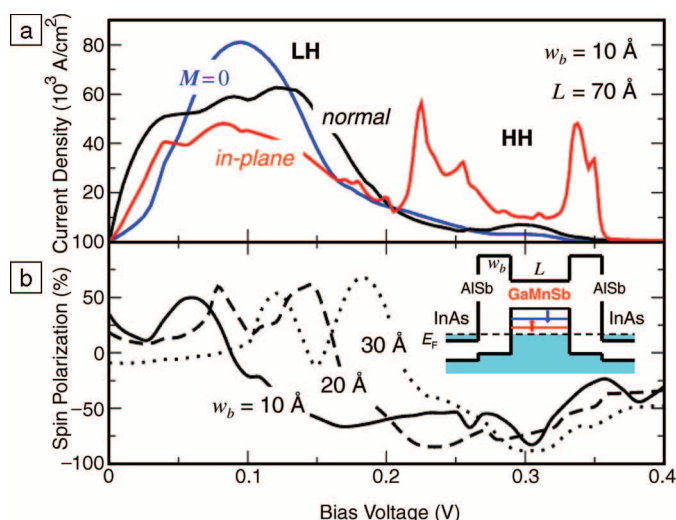


Figure 6. (a) Current-voltage characteristics and (b) spin polarizations of the transmitted current for InAs/AlSb/GaMnSb-based spin resonant interband tunneling diodes (spin-RITDs). Inset: schematic flat-band diagram of InAs/AlSb/GaMnSb-based spin-RITD. Here E_F is the Fermi energy; L and w_b are the quantum-well width and barrier width, respectively; M is the magnetization; and LH and HH stand for the light hole and heavy hole resonant channels, respectively.

90% (Figure 6b). Also notable is a sharp dependence of the spin polarization on applied bias, which allows for control of both the *magnitude* and *sign* of the polarization by varying an external voltage. This controllable spin filtering is a remarkable feature of spin-RITDs and may have significant potential for a variety of possible spintronic applications.²

Previous investigations of conventional (i.e., spin-independent) interband resonant tunneling have mainly focused on RITDs with GaSb QWs⁸⁵ and reveal quite robust operation in a wide temperature range. Spin-filtering—or more precisely, the exchange splitting of the light-hole channel—has already been observed experimentally in DBHs with semimetallic

ErAs QWs.⁸⁰ Ga_{1-x}Mn_xSb random alloys with Curie temperatures of up to ~30 K have been grown,⁸⁶ and much higher Curie temperatures have been reported for Ga_{1-x}Mn_xSb digital alloys, although this has been attributed to the formation of quasi two-dimensional MnSb islands.⁸⁷ At the same time, digital growth techniques have proven to be very efficient for

Appendix: Modeling Spin Injection Using an Effective Resistor Network

The results of Rashba's theory¹ on the effect of conductivity on spin injection can be illustrated by means of a simplified equivalent resistor network model, shown in the Figure. The model describes a near-contact region with nonequilibrium spins where the electrochemical potentials ζ_{\uparrow} and ζ_{\downarrow} of spin-up and spin-down electrons are significantly different.² The interface contact resistances Σ_{\uparrow}^{-1} and Σ_{\downarrow}^{-1} are introduced as discontinuities of ζ_{\uparrow} and ζ_{\downarrow} at the interface.^{1,3} It can be shown that $\Delta\xi = \xi_{\uparrow} - \xi_{\downarrow}$ obeys the diffusion equation and decays exponentially from the interface into the bulk ferromagnetic and semiconductor regions with characteristic spin diffusion lengths L_F and L_N , respectively.¹⁻³ The spin-up and spin-down currents $I_{\uparrow}(x)$ and $I_{\downarrow}(x)$ also depend on x exponentially near the interface, while the total current $I = I_{\uparrow} + I_{\downarrow} = \text{constant}$.

In the effective resistor network model, we replace the near-interface region $L_F + L_N$ with the equivalent resistances that are connected in parallel, as shown in the

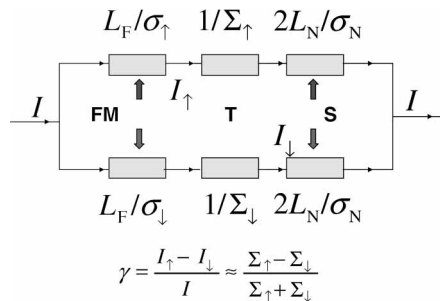


Figure. Equivalent resistor network illustrating spin-injection from a ferromagnet into a semiconductor.

Figure. The equivalent resistances are expressed as L/σ , where σ is the relevant conductivity, and a factor of two appears in each channel of the semiconductor (normal) region since the conductivity of the semiconductor is $\sigma_N/2$ per spin channel. Thus, the nonuniform currents $I_{\uparrow}(x)$ and $I_{\downarrow}(x)$ are replaced by their values $I_{\uparrow}(0)$ and $I_{\downarrow}(0)$ at the interface. As a result, the spin-injection coefficient $\gamma = [I_{\uparrow}(0) - I_{\downarrow}(0)]/I$ and junction resistance $R_j = R_{\text{tot}} - (L_F/\sigma_F + L_N/\sigma_N)$ are reproduced exactly. Here, $\sigma_F = \sigma_{\uparrow} + \sigma_{\downarrow}$ and σ_N are the conductivities of the ferromagnetic metal and semiconductor, respectively, and R_{tot} is the total resistance of the nonequilibrium spin-accumulation region of length $L_F + L_N$.

The quantities γ and R_j can be calculated straightforwardly from the Figure (see Equations 18 and 21 in Rashba's paper, Reference 1). For example,

$$\gamma = \frac{I_{\uparrow} - I_{\downarrow}}{I} = \frac{L_F/\sigma_{\downarrow} - L_F/\sigma_{\uparrow} + 1/\Sigma_{\downarrow} - 1/\Sigma_{\uparrow}}{L_F/\sigma_{\downarrow} + L_F/\sigma_{\uparrow} + 1/\Sigma_{\downarrow} + 1/\Sigma_{\uparrow} + 4L_N/\sigma_N} = \frac{r_F}{r_F + r_N + r_c} \frac{\sigma_{\uparrow} - \sigma_{\downarrow}}{\sigma_{\uparrow} + \sigma_{\downarrow}} + \frac{r_c}{r_F + r_N + r_c} \frac{\Sigma_{\uparrow} - \Sigma_{\downarrow}}{\Sigma_{\uparrow} + \Sigma_{\downarrow}}, \quad (1a)$$

where

$$r_F = L_F \frac{\sigma_{\uparrow} + \sigma_{\downarrow}}{4\sigma_{\uparrow}\sigma_{\downarrow}}, \quad (1b)$$

$$r_c = \frac{\Sigma_{\uparrow} + \Sigma_{\downarrow}}{4\Sigma_{\uparrow}\Sigma_{\downarrow}}, \quad (1b)$$

and

$$r_N = \frac{L_N}{\sigma_N} \quad (1c)$$

are the effective resistances of the ferromagnet, contact, and semiconductor, respectively. This is exactly Rashba's formula. The first term is not significant if the ferromagnet is a metal rather than a half-metal because of the factor

$$r_F/(r_F + r_N + r_c) \ll 1. \quad (1d)$$

The second term will be significant only if the first fraction is close to 1, that is, only if $r_c \gg r_N, r_F$, and the second fraction is not zero (Σ is spin-selective). The junction resistance can be calculated in the same way.

Hence, two criteria must be satisfied in order to have efficient spin injection: (1) the mesoscopic contact resistance,

$$r_c = (\Sigma_{\uparrow} + \Sigma_{\downarrow})/4\Sigma_{\uparrow}\Sigma_{\downarrow}, \quad (2)$$

must dominate; and (2) the contact must be spin-selective. The spin injection can then be detected either in optical experiments as described earlier or in spin-valve experiments on ferromagnet/semiconductor/ferromagnet junctions in the regime where spin-flip processes in the interior semiconductor region can be neglected, that is, when the width of this region is smaller than the spin diffusion length

($w \ll L_N$) and the contact resistance is not too large:³

$$(L_N/\sigma_N \ll r_c \ll L_N^2/\sigma_N w). \quad (3)$$

References

1. E.I. Rashba, *Phys. Rev. B* **62** (2000) p. R16267.
2. P.C. van Son, H. van Kempen, and P. Wyder, *Phys. Rev. Lett.* **58** (1987) p. 2271.
3. A. Fert and H. Jaffres, *Phys. Rev. B* **64** 184420 (2001) □

growing high-quality magnetic QWs.⁸⁸ These developments may soon make the manufacturing of the spin-RITD a reality.

Acknowledgments

This work was supported by the Defense Advanced Research Projects Agency "Spins in Semiconductors" program. B.T. Jonker and S.C. Erwin further acknowledge support from the Office of Naval Research. A. Petrou acknowledges support from the National Science Foundation. A.G. Petukhov acknowledges financial support from the Naval Research Laboratory through the ASEE–Navy Summer and Sabbatical Leave programs, and from NSF grant DMR-0071823. The authors thank the many people who have contributed to the work presented here, including A.T. Hanbicki, G. Kioseoglou, Y.D. Park (now at Seoul National University), and R.M. Stroud at NRL; G. Itskos, R. Mallory, and M. Yasar at the University of Buffalo; and former South Dakota School of Mines and Technology students D. Demchenko (now at Georgetown University) and A. Chantis (now at Arizona State University).

References


1. H.S.P. Wong, D.J. Frank, P.M. Solomon, C.H.J. Wann, and J.J. Welser, *Proc. IEEE*, Vol. 87 (Institute of Electrical and Electronics Engineers, Piscataway, NJ, 1999) p. 537.
2. S.A. Wolf, D.D. Awschalom, R.A. Buhrman, J.M. Daughton, S. von Molnár, M.L. Roukes, A.Y. Chtchelkanova, and D.M. Treger, *Science* **294** (2001) p. 1488.
3. B.T. Jonker, *Proc. IEEE*, Vol. 91 (Institute of Electrical and Electronics Engineers, Piscataway, NJ, 2003) p. 727.
4. D.P. DiVincenzo, *Science* **269** (1995) p. 255.
5. S. Datta and B. Das, *Appl. Phys. Lett.* **56** (1990) p. 665.
6. P. Bruno and J. Wunderlich, *J. Appl. Phys.* **84** (1998) p. 978.
7. H. Ohno, N. Akiba, F. Matsukura, A. Shen, K. Ohtani, and Y. Ohno, *Appl. Phys. Lett.* **73** (1998) p. 363.
8. E.A. de Andrada e Silva and G.C. La Rocca, *Phys. Rev. B* **59** (1999) p. R15583.
9. T. Hayashi, M. Tanaka, and A. Asamitsu, *J. Appl. Phys.* **87** (2000) p. 4673.
10. Th. Gruber, M. Keim, R. Fiederling, G. Reuscher, W. Ossau, G. Schmidt, L. Molenkamp, and A. Waag, *Appl. Phys. Lett.* **78** (2001) p. 1101.
11. T. Koga, J. Nitta, H. Takayanagi, and S. Datta, *Phys. Rev. Lett.* **88** 126601 (2002).
12. A.F. Morpurgo, J.P. Heida, T.M. Klapwijk, B.J. van Wees, and G. Borghs, *Phys. Rev. Lett.* **80** (1998) p. 1050.
13. J. Nitta, F. Meijer, Y. Narita, and H. Takayanagi, *Physica E* **6** (2000) p. 318.
14. B.T. Jonker, U.S. Patent No. 5,874,749 (February 23, 1999).
15. A.G. Petukhov, A.N. Chantis, and D.O. Demchenko, *Phys. Rev. Lett.* **89** 107205 (2002).
16. D. Hägele, M. Oestreich, W.W. Rühle, N. Nestle, and K. Eberl, *Appl. Phys. Lett.* **73** (1998) p. 1580.
17. J.M. Kikkawa and D.D. Awschalom, *Nature* **397** (1999) p. 139.
18. J.M. Kikkawa and D.D. Awschalom, *Phys. Rev. Lett.* **80** (1998) p. 4313.
19. R.I. Dzhioev, K.V. Kavokin, V.L. Korenev, M.V. Lazarev, B. Ya. Meltser, M.N. Stepanova, B.P. Zakharchenya, D. Gammon, and D.S. Katzer, *Phys. Rev. B* **66** 245204 (2002).
20. Y.Q. Jia, R.C. Shi, and S.Y. Chou, *IEEE Trans. Magn.* **32** (1996) p. 4707.
21. A. Hirohata, Y.B. Xu, C.M. Guertler, J.A.C. Bland, and S.N. Holmes, *Phys. Rev. B* **63** 104425 (2001).
22. J.E. Hirsch, *Phys. Rev. Lett.* **83** (1999) p. 1834.
23. S. Zhang, *Phys. Rev. Lett.* **85** (2000) p. 393.
24. F. Meier and B.P. Zakharchenya, *Optical Orientation* (North-Holland, Amsterdam, 1984).
25. C. Weisbuch and B. Vinter, *Quantum Semiconductor Structures*, Chapter 11 (Academic Press, New York, 1991).
26. J.K. Furdyna and J. Kossut, eds., *Diluted Magnetic Semiconductors, Semiconductors, and Semimetals*, Vol. 25, R.K. Willardson and A.C. Beer, series editors (Academic Press, New York, 1988).
27. M. Jain, *Diluted Magnetic Semiconductors* (World Scientific, Singapore, 1991).
28. R. Fiederling, M. Keim, G. Reuscher, W. Ossau, G. Schmidt, A. Waag, and L.W. Molenkamp, *Nature* **402** (1999) p. 787.
29. B.T. Jonker, Y.D. Park, B.R. Bennett, H.D. Cheong, G. Kioseoglou, and A. Petrou, *Phys. Rev. B* **62** (2000) p. 8180.
30. B.T. Jonker, A.T. Hanbicki, Y.D. Park, G. Itskos, M. Furis, G. Kioseoglou, A. Petrou, and X. Wei, *Appl. Phys. Lett.* **79** (2001) p. 3098. See also *Nature Physics Portal*: "Spintronics Quantified," <http://www.nature.com/physics/highlights/6860-3.html> (accessed July 2003).
31. Y.D. Park, B.T. Jonker, B.R. Bennett, G. Itskos, M. Furis, G. Kioseoglou, and A. Petrou, *Appl. Phys. Lett.* **77** (2000) p. 3989.
32. R.M. Stroud, A.T. Hanbicki, Y.D. Park, G. Kioseoglou, A.G. Petukhov, B.T. Jonker, G. Itskos, and A. Petrou, *Phys. Rev. Lett.* **89** 166602 (2002).
33. T. Dietl, H. Ohno, F. Matsukura, J. Cibert, and D. Ferrand, *Science* **287** (2000) p. 1019.
34. T. Dietl, H. Ohno, and F. Matsukura, *Phys. Rev. B* **63** 195205 (2001).
35. M. Kohda, Y. Ohno, K. Takamura, F. Matsukura, and H. Ohno, *Jpn. J. Appl. Phys., Part 2: Lett.* **40** (2001) p. L1274.
36. E. Johnston-Halperin, D. Lofgreen, R.K. Kawakami, D.K. Young, L. Coldren, A.C. Gossard, and D.D. Awschalom, *Phys. Rev. B* **65** 041306(R) (2002).
37. M. Tanaka and Y. Higo, *Phys. Rev. Lett.* **87** 026602 (2001).
38. S.H. Chun, H.J. Potashnik, K.C. Ku, P. Schiffer, and N. Samarth, *Phys. Rev. B* **66** 100408(R) (2002).
39. Y.D. Park, A.T. Hanbicki, J.E. Mattson, and B.T. Jonker, *Appl. Phys. Lett.* **81** (2002) p. 1471.
40. P.R. Hammar, B.R. Bennett, M.J. Yang, and M. Johnson, *Phys. Rev. Lett.* **83** (1999) p. 203.
41. C.-M. Hu, J. Nitta, A. Jensen, J.B. Hansen, and H. Takayanagi, *Phys. Rev. B* **63** 125333 (2001).
42. S. Gardelis, C.G. Smith, C.H.W. Barnes, E.H. Linfield, and D.A. Ritchie, *Phys. Rev. B* **60** (1999) p. 7764.
43. F.G. Monzon, H.X. Tang, and M.L. Roukes, *Phys. Rev. Lett.* **84** (2000) p. 5022.
44. B.J. van Wees, *Phys. Rev. Lett.* **84** (2000) p. 5023.
45. A.T. Filip, B.H. Hoving, F.J. Jedema, B.J. van Wees, B. Dutta, and S. Borghs, *Phys. Rev. B* **62** (2000) p. 9996.
46. G. Schmidt, D. Ferrand, L.W. Molenkamp, A.T. Filip, and B.J. van Wees, *Phys. Rev. B* **62** (2000) p. R4790.
47. D.L. Smith and R.N. Silver, *Phys. Rev. B* **64** 045323 (2001).
48. A. Fert and H. Jaffres, *Phys. Rev. B* **64** 184420 (2001).
49. Z.G. Yu and M. Flatte, *Phys. Rev. B* **66** 201202(R) (2002).
50. R.A. de Groot, F.M. Mueller, P.G. van Engen, and K.H.J. Buschow, *Phys. Rev. Lett.* **50** (1983) p. 2024.
51. W.E. Pickett and J.S. Moodera, *Phys. Today* **54** (5) (2001) p. 39.
52. D. Orgassa, H. Fujiwara, T.C. Schulthess, and W.H. Butler, *Phys. Rev. B* **60** (1999) p. 13237.
53. E.I. Rashba, *Phys. Rev. B* **62** (2000) p. R16267.
54. R. Meservey and P.M. Tedrow, *Phys. Rep.* **238** (1994) p. 173.
55. J.S. Moodera, L.R. Kinder, T.M. Wong, and R. Meservey, *Phys. Rev. Lett.* **74** (1995) p. 3723.
56. P. Clark, *EE Times* (February 9, 2001) p. 14.
57. M. Ilegems, in *The Technology and Physics of Molecular Beam Epitaxy*, edited by E.H.C. Parker (Plenum Publishers, New York, 1985) p. 119.
58. S.M. Sze, *Physics of Semiconductor Devices*, 2nd ed. (John Wiley & Sons, New York, 1981) p. 294.
59. A.T. Hanbicki, B.T. Jonker, G. Itskos, G. Kioseoglou, and A. Petrou, *Appl. Phys. Lett.* **80** (2002) p. 1240.
60. A.T. Hanbicki, O.M.J. van't Erve, R. Magno, G. Kioseoglou, C.H. Li, B.T. Jonker, G. Itskos, R. Mallory, M. Yasar, and A. Petrou, *Appl. Phys. Lett.* **82** (2003) p. 4092.
61. J.D. Albrecht and D.L. Smith, *Phys. Rev. B* **66** 113303 (2002).
62. H.J. Zhu, M. Ramsteiner, H. Kostial, M. Wassermeier, H.-P. Schönherr, and K.H. Ploog, *Phys. Rev. Lett.* **87** 016601 (2001).
63. M. Ramsteiner, H.Y. Hao, A. Kawaharazuka, H.-J. Zhu, M. Kästner, R. Hey, L. Däweritz, H.T. Grahn, and K.H. Ploog, *Phys. Rev. B* **66** 081304R (2002).
64. T. Manago and H. Akinaga, *Appl. Phys. Lett.* **81** (2002) p. 694.
65. V.N. Motsnyi, J. De Boeck, J. Das, W. Van Roy, G. Borghs, E. Goovaerts, and V.I. Safarov, *Appl. Phys. Lett.* **81** (2002) p. 265.
66. M.I. Dyakonov, V.I. Perel, V.L. Berkovits, and V.I. Safarov, *Sov. Phys. JETP* **40** (1975) p. 950.
67. R. Landauer, *Philos. Mag.* **21** (1970) p. 863.
68. M. Büttiker, Y. Imry, R. Landauer, and S. Pinhas, *Phys. Rev. B* **31** (1985) p. 6207.
69. H.U. Baranger and A.D. Stone, *Phys. Rev. B* **40** (1989) p. 8169.
70. J.M. MacLaren, X.-G. Zhang, W.H. Butler, and X. Wang, *Phys. Rev. B* **59** (1999) p. 5470.
71. S. Sanvito and N.A. Hill, *Phys. Rev. Lett.* **87** 267202 (2001).
72. O. Wunnicke, Ph. Mavropoulos, R. Zeller, P.H. Dederichs, and D. Grundler, *Phys. Rev. B* **65** 241306(R) (2002); O. Wunnicke, P. Mavropoulos, and P.H. Dederichs, *J. Supercond./Novel Magn.* **16** (2003) p. 171.
73. M. Zwierzycki, K. Xia, P.J. Kelly, G.E.W. Bauer, and I. Turek, *Phys. Rev. B* **67** 092401 (2003).

74. B.T. Jonker, in *Ultrathin Magnetic Structures IV: Spintronics*, edited by J.A.C. Bland and B. Heinrich (Springer-Verlag, Berlin) in press.
 75. R.M. Stroud (unpublished).
 76. S.C. Erwin, S.-H. Lee, and M. Scheffler, *Phys. Rev. B* **65** 205422 (2002).
 77. P.C. van Son, H. van Kempen, and P. Wyder, *Phys. Rev. Lett.* **58** (1987) p. 2271.
 78. K.M. Schep, J.B.A.N. van Hoof, P.J. Kelly, G.E.W. Bauer, and J.E. Inglesfield, *Phys. Rev. B* **56** (1997) p. 10805.
 79. S. Datta, *Electronic Transport in Mesoscopic Systems* (Cambridge University Press, Cambridge, 1995).

80. D.E. Brehmer, K. Zhang, Ch.J. Schwarz, S.-P. Chau, S.J. Allen, J.P. Ibbetson, J.P. Zhang, C.M. Palmström, and B. Wilkens, *Appl. Phys. Lett.* **67** (1995) p. 1268; A.G. Petukhov, W.R.L. Lambrecht, and B. Segall, *Phys. Rev. B* **53** (1996) p. 3646.
 81. J.C. Slonczewski, *Phys. Rev. B* **39** (1989) p. 6995.
 82. M. Jullière, *Phys. Lett.* **54A** (1975) p. 225.
 83. D.A. Stewart and M. van Schilfgaarde, *J. Appl. Phys.* **93** (2003) p. 7355.
 84. A.G. Petukhov, D.O. Demchenko, and A.N. Chantis, to appear in *Phys. Rev. B* (2003), preprint available on the arXiv.org archive as

<http://arXiv.org/abs/cond-mat/0211300> (accessed September 2003).

85. R.R. Marquardt, D.A. Collins, Y.X. Liu, Z.-Y. Ting, and T.C. McGill, *Phys. Rev. B* **53** (1996) p. 13624.
 86. F. Matsukura, E. Abe, and H. Ohno, *J. Appl. Phys.* **87** (2000) p. 6442.
 87. X. Chen, M. Na, M. Cheon, S. Wang, H. Luo, B.D. McCombe, X. Liu, Y. Sasaki, T. Wojtowicz, J.K. Furdyna, S.J. Potashnik, and P. Schiffer, *Appl. Phys. Lett.* **81** (2002) p. 511.
 88. S.A. Crooker, D.A. Tulchinsky, J. Levy, D.D. Awschalom, R. Garcia, and N. Samarth, *Phys. Rev. Lett.* **75** (1995) p. 505 □



IUMRS-ICEM
9th International Conference
on Electronic Materials

MRS
2004
SPRING MEETING
SAN FRANCISCO, CA USA

Mark Your Calendar!

2004 MRS Spring Meeting

www.mrs.org/meetings/spring2004/

National Defense Science and Engineering Graduate Fellowship

- ★ **\$27,500 personal stipend for the first year, \$28,000 the second, and \$28,500 the third.**
- ★ **Full Tuition & Fees, Health Insurance Allowance**
- ★ **200 new three year awards expected**
- ★ **No military service obligation**
- ★ **January 9, 2004 application deadline**
- ★ **See website for updates and to apply**

The Department of Defense is committed to increasing the number and quality of American men and women who will lead state-of-the-art research projects in disciplines having the greatest payoff to national security requirements through Fellowships awarded to U.S. citizens or nationals under the National Defense Science and Engineering Graduate Fellowship program. Fellowships are sponsored by the Army Research Office, the Office of Naval Research, the Air Force Office of Scientific Research, and the High Performance Computing Modernization Program.

www.asee.org/ndseg for more info

In accordance with Federal statutes and regulations, no person on the grounds of race color, age, sex, national origin or disability shall be excluded from participating in, denied the benefits of, or be subject to discrimination, under any program activity receiving financial assistance from the Department of Defense.

NDSEG Fellowships are intended for students at or near the beginning of their graduate studies closely related to the following disciplines:

Aeronautical and Astronautical Engineering
 Biosciences
 Chemical Engineering
 Chemistry
 Civil Engineering
 Cognitive, Neural, and Behavioral Sciences
 Computer and Computational Sciences
 Electrical Engineering
 Geosciences
 Materials Science and Engineering
 Mathematics
 Mechanical Engineering
 Naval Architecture and Ocean Engineering
 Oceanography
 Physics
 Several interdisciplinary areas, including acoustics, computer architecture, and nanosciences.

